Article

The Effects on Stability and Electronic Structure of Si-Segregated θ′/Al Interface Systems in Al-Cu Alloys

Lu Jiang [1], Zhihao Zhao [1,*] and Gaosong Wang [1,2]

1 School of Materials Science and Engineering, Northeastern University, Shenyang 110819, China; jianglu0904@163.com (L.J.); wanggs@epm.neu.edu.cn (G.W.)
2 Key Laboratory of Electromagnetic Processing of Materials, Ministry of Education, Northeastern University, Shenyang 110819, China
* Correspondence: zzh@epm.neu.edu.cn

Abstract: This study systematically investigates the energy and electronic properties of Si-segregated θ′(Al_2Cu)/Al semi-coherent and coherent interface systems in Al-Cu alloys using ab initio calculations. By evaluating the bonding strength at the interface, it has been revealed that Si segregated at the A1 site (Al slab) of the semi-coherent interface systems exhibits the most negative segregation energy, resulting in a noticeable decrease in total energy and an increase in interface adhesion. The electronic structure analysis indicates the presence of Al-Cu and Al-Al bonds, with Si occupying the A1 site. The strong bond formation between Al-Cu and Al-Al is essential for improving interface bonding strength. The results of the calculating analyses are consistent with the results of the previous experiments, and Si can be used as a synergistic element to reduce the θ′/Al interface energy and further reduce the coarsening drive of the θ′ precipitated phase, which can provide new perspectives and computational ideas for the compositional design of heat-resistant Al-Cu alloys.

Keywords: θ′/Al interface; first principles; Si segregated; electronic structure; bonding strength

1. Introduction

The Al-Cu alloys have become recognized for their combination of low density, great strength, and excellent high-temperature creep resistance capabilities. They have been extensively employed in the aerospace and civil industries owing to their remarkable overall properties. Over the years, researchers have refined the elemental composition of Al-Cu alloys to develop various Al-Cu series alloys (such as 2618, 2219, and 2124Al alloys) that fulfill various performance requirements. Alloys achieve remarkably high strength and exceptional overall mechanical properties through precipitation strengthening [1–8]. During the aging process, the rapid disintegration of solid solutions leads to the formation of a sequence of precipitate phases at the nano-scale level. The commonly acknowledged primary precipitation sequence for Al-Cu alloys is GPI zones → GPII zones → θ′ (Al_2Cu) → θ (Al_2Cu) phase. The θ′ phase serves as the primary strengthening phase in Al-Cu alloys, exhibiting a semi-coherent or coherent relationship with the Al matrix [9–11]. It has a tetragonal structure with a space group of $I\bar{4}m2$, and its lattice parameters are a = b = 0.404 nm and c = 0.580 nm, respectively. However, the θ′ is a metastable phase that is thermodynamically unstable. It undergoes rapid coarsening at a temperature exceeding 200 °C and transforms into the thermodynamically stable phase θ. The θ phase has an incoherent relationship with the Al matrix, and its presence significantly decreases the mechanical properties of the Al-Cu alloys. Microalloying is a highly effective approach for preventing the enlargement of θ′ phases and enhancing the heat resistance of the alloys, which is accomplished by adding trace alloying elements to enhance the thermal stability of θ′ phases within the Al-Cu alloys. Moreover, microalloying elements are segregated at the θ′/Al interface, which can enhance the thermal stability of the interface, thereby

improving the comprehensive mechanical characteristics and expanding the operational temperature range of Al-Cu alloys.

Silicon (Si) has traditionally been viewed as an impurity element in Al-Cu alloys, leading to the beneficial effects of Si on the alloy being often overlooked. Extensive research has been conducted on the impact of trace amounts of Si on the evolution of precipitation and the performance of Al-Cu alloys. Numerous studies [12–19] have shown that adding small amounts of Si can significantly improve the aging response rate of Al-Cu alloys while refining and evenly distributing the precipitates in the matrix, enhancing the comprehensive mechanical properties, and further improving the heat resistance of Al-Cu alloys. Moreover, Si can serve as an auxiliary element and cooperate with elements such as Sc, Mn, Zr, Er, and Mo [13,20–24] to improve the heat resistance of the Al-Cu alloys. The addition of Si can induce the formation of Si-containing GPB zones, Q phases, and heat-resistant cubic σ ($Al_5Cu_6Mg_2$) phases in the alloys. Si can also be used as a heterogeneous nucleation site for the θ' strengthening phases. In conclusion, the addition of Si accelerates the aging response rate, changes the precipitation sequence of the precipitated phases, promotes the precipitation of the heat-resistant phase, increases the heat-resistant number density, and improves the heat resistance of Al-Cu alloys. The addition of a small amount of Si also has a significant effect on the interface. The first-principles calculations [25,26] indicate that Si segregation at the θ'/Al interface could reduce the interface energy, making θ'/Al more stable and making the Al-Cu alloys have better mechanical properties. However, due to the nanometer scale of the precipitated phases in Al-Cu alloys, it is challenging to experimentally explore the interfacial properties and the mechanisms through which trace elements impact the interface between the precipitated phases and the Al matrix.

In this work, Si-segregated semi-coherent and coherent θ'/Al interface systems with various stacking structures were constructed, and the interface and segregation energies, electronic structures, and bond strength of the individual interface systems were analyzed using first-principles calculations. By calculating and analyzing the interface properties of various stacking structures, this study aims to offer theoretical explanations for experimental phenomena on an atomic scale. In addition, this study also seeks to provide theoretical guidance and insights for understanding the impact of trace amounts of Si on the properties of the θ'/Al interface systems, as well as for the design of other trace-element-enhanced Al-Cu alloys.

2. Methods and Calculation Models

2.1. Calculation Details

All calculations in this study were performed using the Vienna Simulation Package (VASP 5.4). The pseudopotentials for the elements are Al: $3s^23p^1$, Cu: $3d^{10}4p^1$, and Si: $3s^23p^2$. The electronic exchange and correlations were characterized using the GGA-PBE (PBE parameterization of generalized gradient approximation) [27–30]. The cutoff energy was established at 400 eV, and the k-point centered around the gamma points was utilized to sample and obtain a density of 0.02. For the electronic density of states (DOS) calculation, k-point meshes of $4 \times 12 \times 1$ were used for four kinds of semi-coherent interface systems, and $12 \times 12 \times 1$ were used for two kinds of coherent interface systems. The vacuum layer thickness was systematically set to 12.0 Å for all calculation interface systems. The total energy convergence reached a 1.0×10^{-5} eV/atom [31] value during the optimization process [32,33].

There are three key steps in our computational analysis work. Firstly, we constructed different computational models based on the experimental results and the different stacking styles and investigated the interface energy of each configuration, which can be selected as a more stable configuration for the next calculation. Secondly, the total energy, interface energy, interface adhesion, and electronic structure of Si segregated at the different slab sites are calculated to derive the preferred occupancy sites. Finally, it is confirmed that Si atoms can be used as a synergistic element to reduce the interface energy and improve the stability of θ'/Al interface systems.

2.2. Interface Properties

2.2.1. Pure Interface Models

In this work, representative θ′/Al interface systems were constructed. The semi-coherent interface systems included six Al layers and seven θ′ layers, while the coherent θ′(001)/Al(001) interfaces included six Al layers and six θ′ layers. These systems were constructed based on results in previous reports [30]. Due to the variations in lattice parameters between Al-slab and θ′-slab, it is crucial to consider the lattice mismatch at the interface while constructing the θ′/Al interface systems. There is a common belief that if the mismatch is below 5% [34], the interface system tends to be more reliable. Regarding the semi-coherent θ′/Al interface systems, the θ′(010) surface and the Al(010) surface have a lattice mismatch of about 35% in the a-direction. This mismatch can be reduced by elongating the a-direction slab to meet the experimental and computational requirements, where the expansion ratio is a ≈ 3aAl ≈ 2aθ′. The lattice parameter at the θ′(001)/Al(001) coherent interface is approximately aAl ≈ aθ′, which has a minimal mismatch. When constructing the surface system, each layer of the θ′(010) surface is terminated by two types of atoms. In contrast, the termination of each layer of the θ′(001) surface by one of the Al or Cu atoms, resulting in two termination modes, needs to be considered. Finally, six interface systems (θ′(010)/Al(010)-top, θ′(010)/Al(010)-hollow, θ′(001)-Al/Al(001)-top, θ′(001)-Al/Al(001)-bridge, θ′(001)-Cu/Al (001)-top, θ′(001)-Cu/Al(001)-bridge) were constructed based on the different surface stacking modes, as depicted in Figure 1a−f.
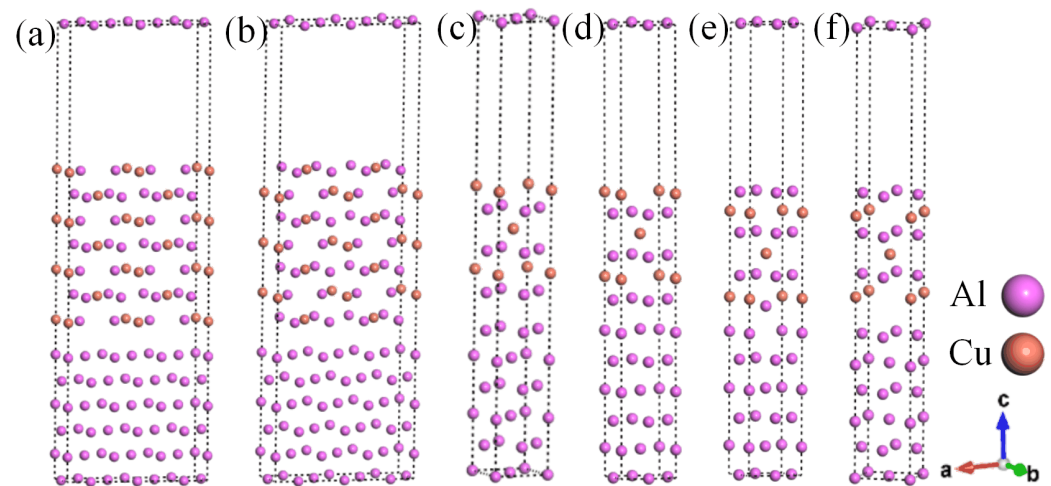
Figure 1. Semi-coherent and coherent θ′/Al interface systems: (**a**) θ′(010)/Al(010)-top interface; (**b**) θ′(010)/Al(010)-hollow; (**c**) θ′(001)-Al/Al(001)-top interface; (**d**) θ′(001)-Al/Al(001)-bridge interface; (**e**) θ′(001)-Cu/Al(001)-top interface; (**f**) θ′(001)-Cu/Al(001)-bridge interface.

2.2.2. Pure Interface Adhesion

Pure interface adhesion (W_{ad}) is the value of energy per area required to divide the θ′/Al interface systems into two distinct surfaces: the θ′ surface and the Al surface. This parameter correlates with the bond strength at the interface systems, which can be applied to estimating the comprehensive mechanical properties of Al-Cu alloys. It is commonly understood that a higher interface adhesion indicates a more robust bond strength at the interface. The formula for the work of adhesion (W_{ad}) is as follows [35,36]:

$$W_{ad} = \frac{E_{slab}^{Al} + E_{slab}^{\theta'} - E_{\theta'/Al}}{A_{int}} \tag{1}$$

where E_{slab}^{Al}, $E_{slab}^{\theta'}$, and $E_{\theta'/Al}$ represent the total energies of the Al-slab, θ′-slab, and θ′/Al interface, and A_{int} represents the total area of the interface systems. The "vacuum partitioning" approach [7] was adopted to calculate $E_{\theta'/Al}$, E_{slab}^{Al}, and $E_{slab}^{\theta'}$, as shown in Figure 2 (taking Cu-terminated θ′(001)-Cu/Al(001) as an example). Firstly, the equilibrium interface

system was obtained through a fully relaxed structural optimization method, followed by a 12 Å vacuum layer applied to the target interface. Sequentially, surface supercells containing Al and θ′ bulks were constructed on the basis of the interface and maintained the vacuum layers as shown in Figure 2b,c.
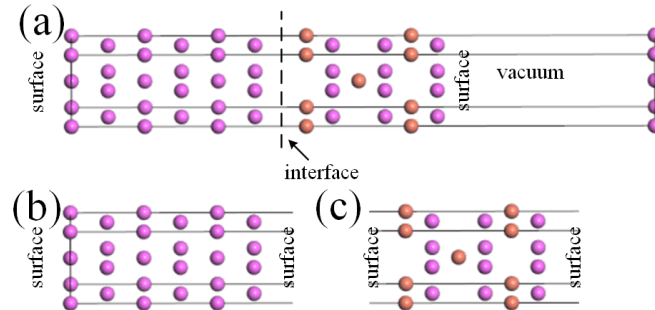
Figure 2. Surface energy solving for θ′/Al interface systems using the "vacuum partitioning" approach: (**a**) Cu-terminated θ′(001)-Cu/Al(001); (**b**) Al-slab structure; (**c**) θ′-slab structure.

2.2.3. Interface Energy

To elucidate the differences in nucleation and growth of the θ′ phase of different interface systems from a heterogeneous nucleation perspective, we calculated the interface energy of six different interface systems. Interface energy refers to the energy value involved in forming an interface through the combination of bulk materials (Al-bulk and θ′-bulk). There is a common belief that lower interface energy means a more stable interface system. Therefore, it is essential to calculate the interface energy of systems, which will be used to select more stable interface systems to construct the Si-segregated interfaces. The interface energy is judged as follows:

$$\gamma_{\text{int}} = \frac{E_{\text{int}} - n_{\text{Al}}E_{\text{Al}}^{\text{bulk}} - n_{\theta'}E_{\theta'}^{\text{bulk}}}{A_{\text{int}}} - \sigma_{\text{Al}} - \sigma_{\theta'} \quad (2)$$

In the equation, E_{int} represents the total energy value of the interface systems, $E_{\text{Al}}^{\text{bulk}}$ and $E_{\theta'}^{\text{bulk}}$ represent the total energy values per Al-bulk and θ′-bulk, respectively, and n represents the number of various bulk materials (Al and θ′) at the interface. σ represents the surface energy values of various slabs (Al-slab and θ′-slab), which are defined as follows [35,36]:

$$\sigma_{\theta'} = \frac{E_{\text{slab}}^{\theta'} - n_{\text{Cu}}E_{\text{Cu}} - \frac{n_{\text{Al}}}{2}\left(\frac{E_{\text{bulk}}^{\theta'}}{n_{\theta'}} - E_{\text{Cu}}\right)}{2A_{\text{surf}}} \quad (3)$$

In the equation, $E_{\text{slab}}^{\theta'}$ represents the total energy value of the θ′-slab with vacuum space, respectively. $E_{bulk}^{\theta'}$ represents the energy values per θ′-bulk, E_{Cu} represents the energy values of Cu atoms in the Cu-bulk, n_{slab} represents the number of Al atoms in the slab, n represents the number of various atoms in the materials, and A_{surf} represents the area of the surface.

Figure 3 represents the interface energy values of six different interface systems. For the semi-coherent interface systems, the values of interface energy for the θ′(010)/Al(010)-top and θ′(010)/Al(010)-hollow systems are 0.59 J/m^2 and 0.61 J/m^2, respectively, which is highly consistent with the experimental findings, demonstrating the reasonability of constructed semi-coherent interface systems. In the coherent interface systems, the interface energy values of top and bridge stacking for the θ′(001)-Al/Al(001) and θ′(001)-Cu/Al(001) interface systems are 0.94 J/m^2, 0.82 J/m^2, 0.47 J/m^2, and 0.57 J/m^2, respectively, where θ′(001)-Cu/Al(001)-bridge has the lowest interface energy, which agrees well with the experimental results [37]. The analysis indicates that the coherent (001)-Cu/Al(001)-bridge is the most stable interface system.
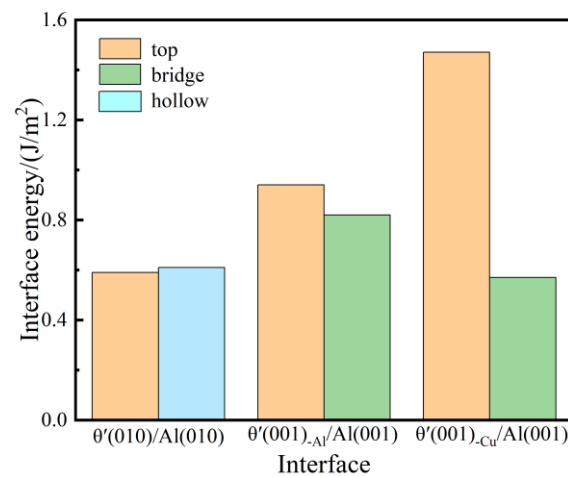
Figure 3. Interface energy value of semi-coherent and coherent θ′/Al interface systems with top, bridge, and hollow site stacking.

Based on the above analysis of results and experimental results [37,38], three systems with θ′(010)/Al(010)-top, θ′(010)/Al(010)-hollow, and θ′(001)-Cu/Al(001)-bridge stacking were selected to construct the Si-segregated interface systems. There are two different segregating situations for Si, which are Al-slab (A1 site) and θ′-slab (A2 site). Therefore, six Si-segregated interfaces were constructed, as depicted in Figure 4.
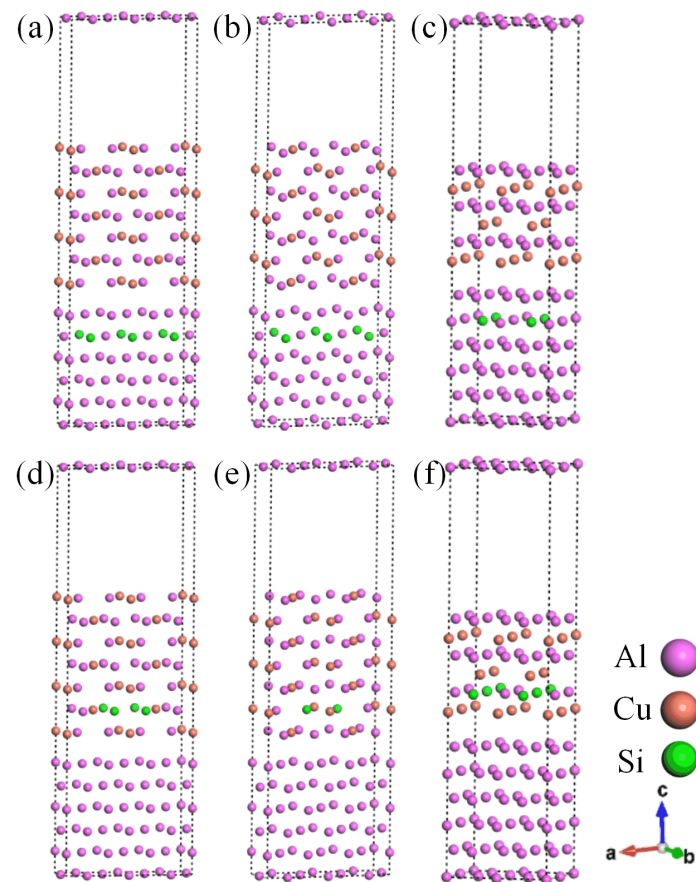
Figure 4. Si-segregated θ′/Al interfaces: (**a**) θ′(010)/Al(010)-top with Si at A1 site interface; (**b**) θ′(010)/Al(010)-hollow with Si at A1 site interface; (**c**) θ′(001)-Cu/Al(001)-bridge with Si at A1 site interface; (**d**) θ′(010)/Al(010)-top with Si at A2 site interface; (**e**) θ′(010)/Al(010)-hollow with Si at A2 site interface; (**f**) θ′(001)-Cu/Al(001)-bridge with Si at A2 site interface.

2.2.4. Segregation Energy

The segregation energy is defined as the energy value necessary for solute atoms to segregate at the θ′/Al interface systems, and its magnitude indicates the strength of the interface systems. A lower value of segregation energy signifies a more substantial capacity of solute atoms to segregate at the θ′/Al interface systems, which can enhance the bonding of interface systems. The segregation energy is defined as follows:

$$E_{\text{seg}} = \left(E_{\text{Al}/\theta'-\text{Si}} - E_{\text{Al}/\theta'} \right) - \left(E_{\text{Si}}^{\text{bulk}} - E_{\text{Al}}^{\text{bulk}} \right) \tag{4}$$

where $E_{Al/\theta'}$ and $E_{Al/\theta'-Si}$ are the total energy values of the pure and Si-segregated interface systems, and E^{bulk} represents the energy value per Al atom and Si atom in bulk materials.

3. Results and Discussion

3.1. Interface Adhesion

Interface adhesion values of the pure and Si-segregated interface systems are illustrated in Figure 5. Interface adhesion values of Si-segregated interface systems show an increase compared to pure interface systems. In particular, the work of adhesion values of Si-segregated interfaces with Si at the A1 site are more significant than those of Si at the A2 site, which indicates that Si segregation can effectively enhance the bonding strength of interface systems. Furthermore, it appears that Si atoms have a strong tendency to segregate at the Al-slab. Furthermore, it is evident that the work of adhesion values of the θ′(010)/Al(010) interface with Si at the A1 site are significantly greater compared to other interface systems, which indicates that Si segregation has the most significant impact on the bond strength of semi-coherent interfaces, resulting in stronger interface adhesion. For pure interface systems, the work of adhesion values of coherent interface systems are greater than those of semi-coherent interfaces. For the Si-segregated interface systems, the work of adhesion values of semi-coherent interfaces with Si at the A1 site interfaces are larger than those of coherent interfaces, while the work of adhesion values of coherent interfaces with Si at the A2 site are extensive compared to semi-coherent interfaces.
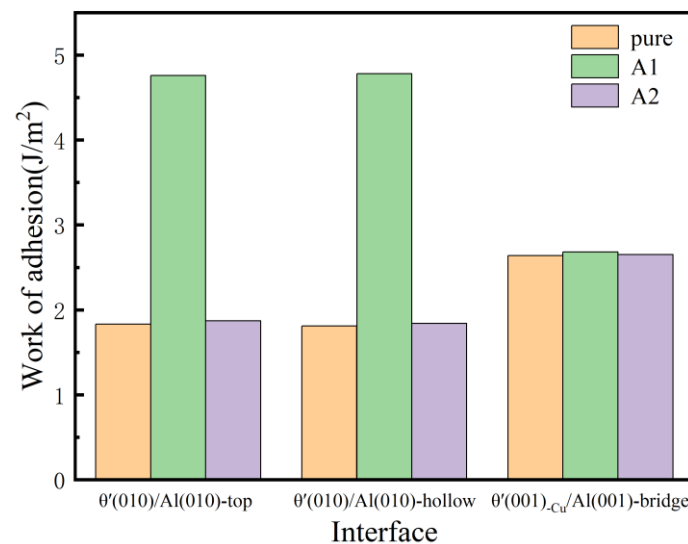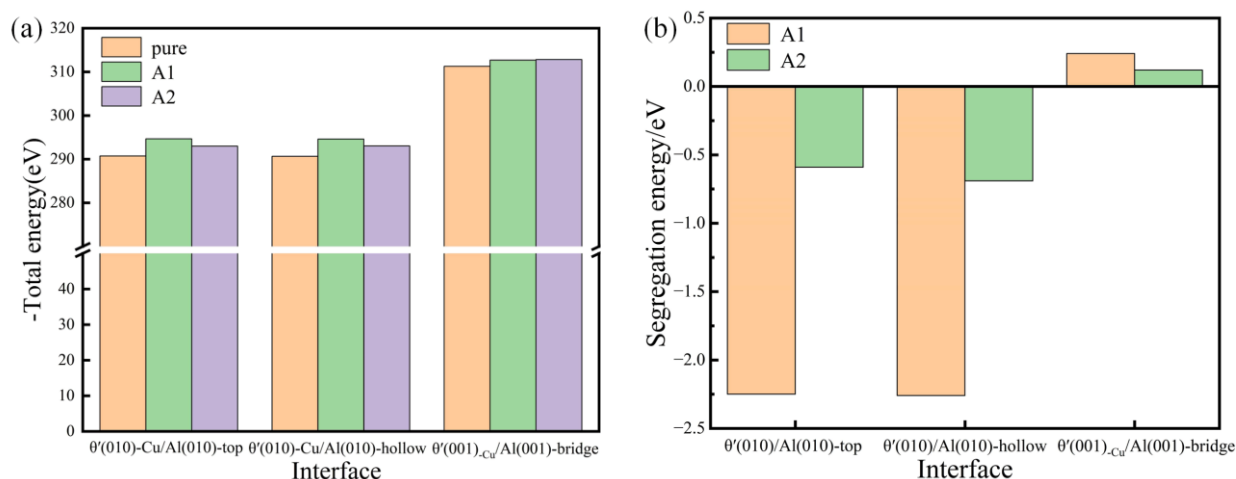

Figure 5. Work of adhesion of pure and Si-segregated interface systems with θ′(001)/Al(001) and θ′(010)/Al(010) interface systems.

3.2. Segregation Energy

The calculation of both the segregation energy and total energy of Si-segregated interface systems was carried out, as depicted in Figure 6. It is obvious that the total energy values of Si-segregated interface systems are lower, indicating that Si segregation can improve the stability of interface systems. The segregation energy values of semi-coherent

interface systems are notably negative compared to coherent interfaces, indicating that the Si segregation ability in semi-coherent systems is significantly greater than in coherent systems. In particular, for the semi-coherent systems, it is evident that the segregation energy values of Si segregated at the A1 site are significantly more negative than those of Si segregated at the A2 site, indicating a much stronger segregation ability at the A1 site. It is further illustrated that the semi-coherent interface systems with Si segregated at the A1 site are the most favorable for interface bonding, aligning well with the interface adhesion results.

Figure 6. Total energy (**a**) and segregation energy (**b**) of pure and Si-segregated interface systems with $\theta'(001)/Al(001)$ and $\theta'(010)/Al(010)$ interfaces.

Based on the above analysis of the interface adhesion, total energy, and segregation energy of the systems, it is evident that Si segregated at the A1 site of semi-coherent interface systems can increase the interface adhesion, reduce the total energy, and improve the stability of the interface systems. These findings are consistent with the reported experimental results [13,15–17].

3.3. Electronic Structure

The atom bond strength at the interface significantly impacts the interface bonding strength. Various analyses were conducted to further explain the effects of Si segregation on the interface strength. These include calculating the ELF (0-1) distribution diagrams to determine the type and strength of chemical bonds, the Bader charge ("+" means gain of electrons, "-" means loss of electrons) to analyze the amount of charge transfer, and the TDOS and PDOS to analyze atomic bonding orbitals.

The ELF value is a numerical measure that falls within the range of 0 to 1. When the ELF value is 1, it signifies complete electron localization. The lowest value, ELF = 0, indicates complete electron delocalization, while ELF = 0.5 represents that electrons at the location can form a distribution of electron pairs similar to an electron gas. Figure 7 exhibits the ELF distributions of pure and Si-segregated interface systems using the {010} cutting plane. The electron localization is significantly enhanced at the Si-segregated interfaces compared to the pure interface systems, indicating a reinforcement of interactions at interface atomic bonding. From Figure 7a–f, we can see that, regarding the semi-coherent systems, the electrons around Al and Cu atoms from Al-slab and θ'-slab are localized, forming the Al-Cu bond with stronger bond strength. Moreover, a weaker Al-Al bond is formed between Al and Al atoms in the Al-slab and θ'-slab. From Figure 7a, we observe that the Al atoms at the interface of the Al-slab (Al-Cu bond) lose 0.4 e and 0.1 e, respectively. Similarly, in Figure 7d, the Al atoms at the Al-slab (Al-Al bond) gain 0.2 e and 0.06 e, respectively. The Bader charge shows that the number of charge transfers between Al-Cu atoms at the interface is more significant than that of Al-Al atoms, suggesting the Al-Cu

bond is stronger. The finding agrees with the ELF distribution analysis. From Figure 7g–i, we can see that regarding the coherent interfaces, the ELF distribution value between Al and Al atoms from Al-slab and θ′-slab is approximately 0.6, indicating the formation of the Al-Al bond.
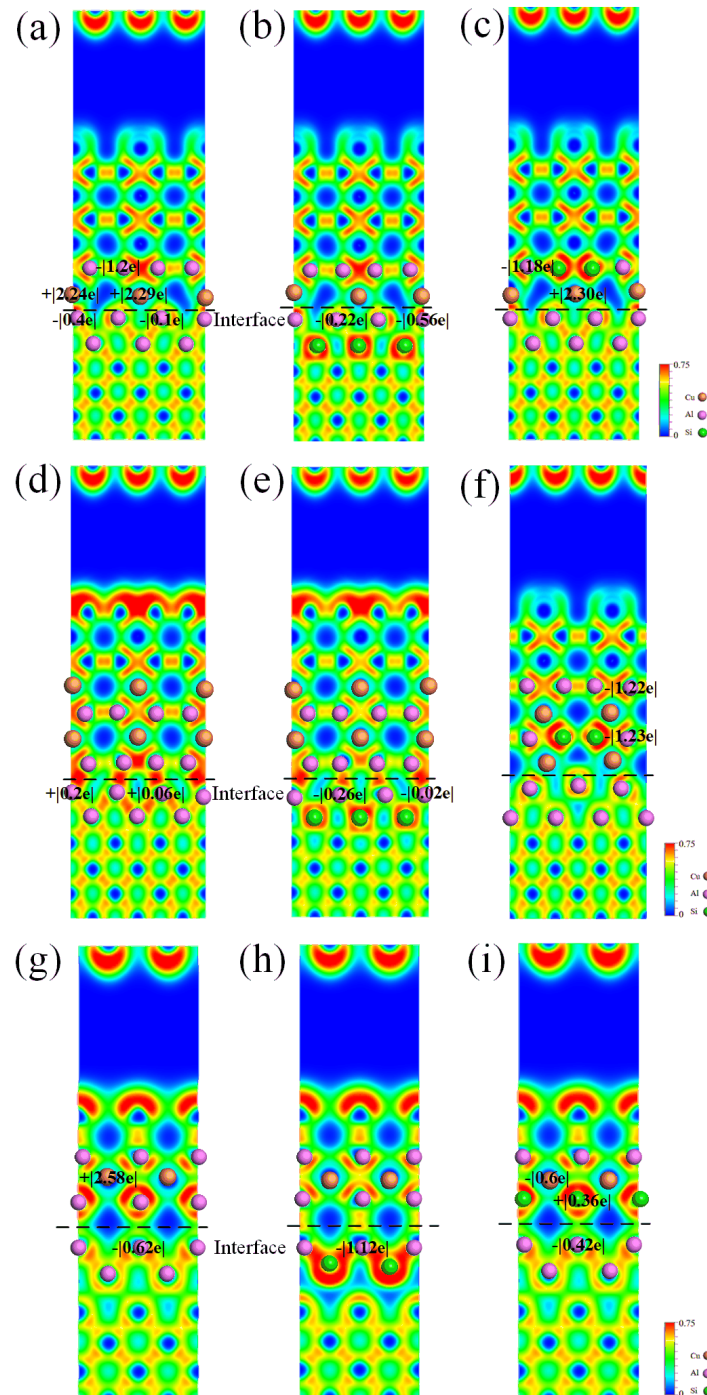

Figure 7. Electron localization function (ELF) distributions and Bader charge values of pure and Si-segregated interface systems: (**a**) θ′(010)/Al(010)-top interface; (**b**) θ′(010)/Al(010)-top with Si at A1 site interface; (**c**) θ′(010)/Al(010)-top with Si at A2 site interface; (**d**) θ′(010)/Al(010)-hollow interface; (**e**) θ′(010)/Al(010)-hollow with Si at A1 site interface; (**f**) θ′(010)/Al(010)-hollow with Si at A2 site interface; (**g**) θ′(001)-Cu/Al(001)-bridge interface; (**h**) θ′(001)-Cu/Al(001)-bridge with Si at A1 site interface; (**i**) θ′(001)-Cu/Al(001)-bridge with Si at A2 site interface.

Additionally, a less strong Al-Cu bond is formed. The atomic bond interactions between Al and Al at the interface with Si at the A1 site are significantly stronger compared to those with Si at the A2 site, according to the analysis of ELF distributions and Bader charge values. This finding explains the above calculation, demonstrating that the interface systems in which Si atoms are segregated at the A1 site exhibit higher work of adhesion and more negative segregation energy than those with Si at the A2 site.

To further reveal the bonding orbitals between atoms, the TDOS and PDOS of pure and Si-segregated interface systems were calculated, which are shown in Figure 8. The analysis reveals that below the Fermi energy level, the Al-Cu atomic bond has significant orbital hybridization interactions, indicating the formation of the Al-Cu bond. For the Si-segregated interfaces, hybridization is observed among Al-p, Cu-d, and Si-p orbits, which appear with some overlapping peaks. Particularly at the interfaces with Si at the A1 site, Al-p and Cu-d have a noticeable hybridization, contributing to the formation of Al-Cu bonds. Through the comprehensive analysis of ELF distributions and Bader charge values, it can be inferred that the presence of significant Al-Cu and Al-Al bonds in Si-segregated systems significantly enhances the interface bonding strength.
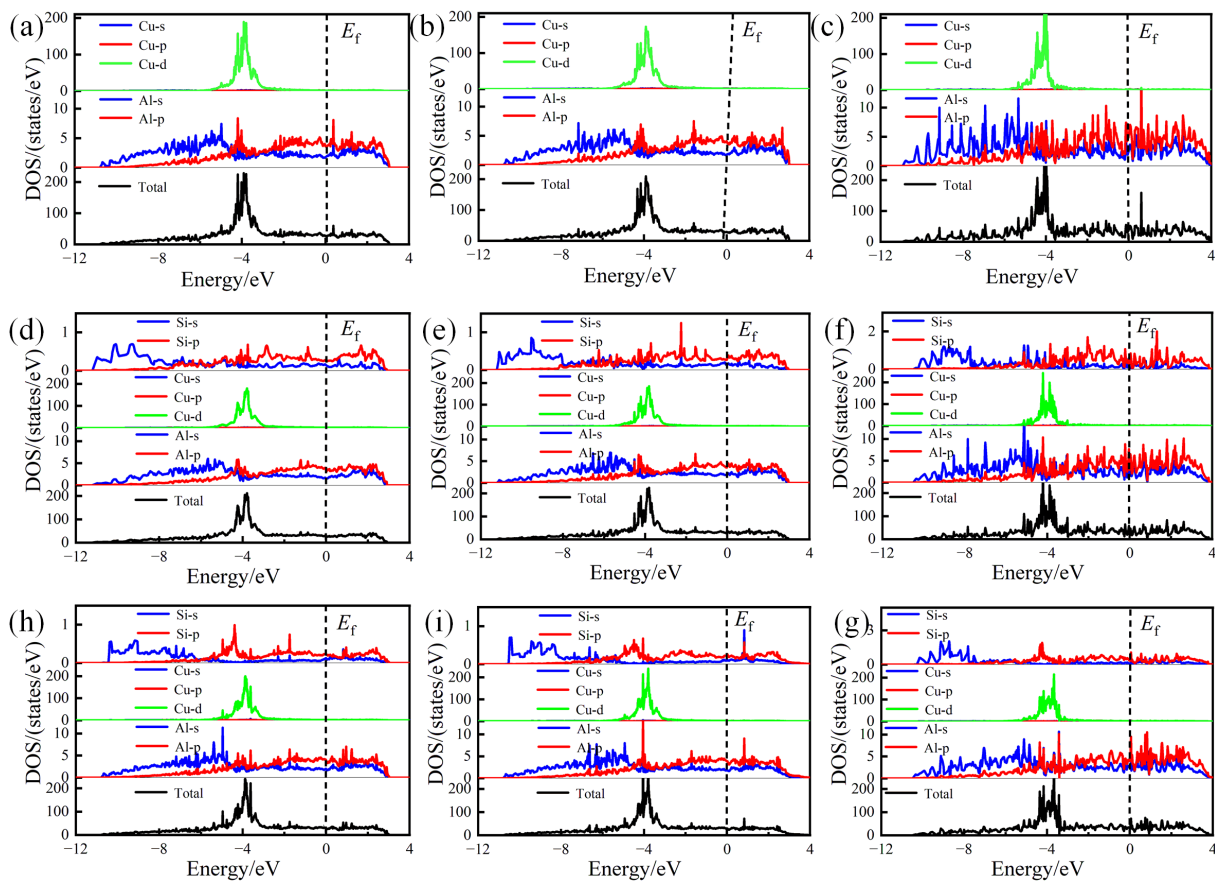
Figure 8. Total electronic density of states (TDOS) and partial electronic density of states (PDOS) of pure and Si-segregated interface systems: (**a**) θ′(010)/Al(010)-top interface; (**b**) θ′(010)/Al(010)-hollow interface; (**c**) θ′(001)-Cu/Al(001)-bridge interface; (**d**) θ′(010)/Al(010)-top with Si at A1 site interface; (**e**) θ′(010)/Al(010)-hollow with Si at A1 site interface; (**f**) θ′(001)-Cu/Al(001)-bridge with Si at A1 site interface; (**g**) θ′(010)/Al(010)-top with Si at A2 site; interface (**h**) θ′(010)/Al(010)-hollow with Si at A2 site interface; (**i**) θ′(001)-Cu/Al(001)-bridge with Si at A2 site interface.

4. Conclusions

In this work, various energies, interface adhesion, and electronic structures of Si-segregated θ′/Al interface systems have been carried out through first-principles calculations. The main conclusions are as follows:

1. Si segregation has a significant impact on the θ′/Al semi-coherent and coherent interface energy and bond strength. It can reduce the total energy, increase the interface adhesion, improve the stability of interface systems, and reduce the coarsening drive of the θ′ precipitation phase.
2. Si segregation can significantly enhance the bond strength of the θ′/Al interface systems. It promotes the hybridization of Al-Al and Al-Cu orbitals, resulting in enhanced hybridization between them, which is the essential reason for enhancing interface bonding strength.
3. Si atoms exhibit a greater tendency to segregate at the Al-slab compared to the θ′-slab, and semi-coherent interface systems with Si at the A1 site have the highest work of adhesion, the most negative segregation energy, and stronger bonding strength.

This study provides an insight into the electronic structure stability of the θ′ phases and the θ′/Al interface on an atomic scale, which can be used as a knowledge base for the design of heat-resistant Al-Cu alloys. This will be beneficial for the improvement and enhancement of the heat resistance of new Al-Cu alloys.

Institutional Review Board Statement: Not applicable.

Informed Consent Statement: Not applicable.

Data Availability Statement: Data are contained within this article.

Conflicts of Interest: The authors declare no conflicts of interest.

References

1. Esteban-Manzanares, G.; Martínez, E.; Segurado, J.; Capolungo, L.; LLorca, J. An atomistic investigation of the interaction of dislocations with guinier-preston zones in Al-Cu alloys. *Acta Mater.* **2019**, *162*, 189–201. [CrossRef]
2. Yang, H.; Tian, S.; Gao, T.; Nie, J.; You, Z.; Liu, G.; Wang, H.; Liu, X. High-temperature mechanical properties of 2024 Al matrix nanocomposite reinforced by TiC network architecture. *Mater. Sci. Eng. A* **2019**, *763*, 138121. [CrossRef]
3. Sun, D.; Wang, Y.; Lu, Y.; Chen, Z.; Rao, Q. Influence of atom termination and stacking sequence on the θ′/Al interfaces from first-principles calculations. *Superlattices Microstruct.* **2016**, *94*, 215–222. [CrossRef]
4. Saurabh, G.; Jayaganthan, R.; Joe, A. Laser powder bed fusion on Ti modified Al 2024 alloy: Influence of build orientation and T6 treatment on mechanical behaviour, microstructural features and strengthening mechanisms. *Mater. Sci. Eng. A* **2024**, *896*, 146296.
5. Bahramyan, M.; Mousavian, R.T.; Brabazon, D. Molecular dynamic simulation of edge dislocation-void interaction in pure Al and Al-Mg alloy. *Mater. Sci. Eng. A* **2016**, *674*, 82–90. [CrossRef]
6. Liu, L.; Chen, J.H.; Wang, S.B.; Liu, C.H.; Yang, S.S.; Wu, C.L. The effect of Si on precipitation in Al–Cu–Mg alloy with a high Cu/Mg ratio. *Mater. Sci. Eng. A* **2014**, *606*, 187–195. [CrossRef]
7. Wang, S.; Zhang, C.; Li, X.; Wang, J. Uncovering the influence of Cu on the thickening and strength of the δ′/θ′/δ′ nano-composite precipitate in Al–Cu–Li alloys. *J. Mater. Sci.* **2021**, *56*, 10092–10107. [CrossRef]
8. Poplawsky, J.D.; Michi, R.A.; Allard, L.F.; Bahl, S.; Plotkowski, A.J.; Shyam, A. Using θ′ interfaces as templates for planar L12 precipitation in AlCuMnZr alloys. *Addit. Manuf. Lett.* **2022**, *3*, 100086. [CrossRef]
9. Li, C.; Guo, R.; He, S.; Xuan, W.; Li, X.; Zhong, Y.; Ren, Z. Formation of novel microstructures in quenched Al Cu alloys in steady magnetic field. *J. Alloys Compd.* **2019**, *776*, 353–356. [CrossRef]
10. Wang, L.; Lu, W.; Hu, Q.; Xia, M.; Wang, Y.; Li, J.G. Interfacial tuning for the nucleation of liquid AlCu alloy. *Acta Mater.* **2017**, *139*, 75–85. [CrossRef]
11. Li, Q.; Zhang, Y.; Lan, Y.; Zhang, Y.; Xia, T. The effect of Sc addition on the novel nano-AlCu phase in as-cast Al-5%Cu alloy. *J. Alloys Compd.* **2020**, *831*, 154739. [CrossRef]
12. Xiao, Q.; Liu, H.; Yi, D.; Yin, D.; Chen, Y.; Zhang, Y.; Wang, B. Effect of Cu content on precipitation and age-hardening behavior in Al-Mg-Si-xCu alloys. *J. Alloys Compd.* **2017**, *695*, 1005–1013. [CrossRef]
13. Liang, S.S.; Ma, J.R.; Guo, K.H.; Wen, S.P.; Wei, W.; Wu, X.L.; Huang, H.; Gao, K.Y.; Liu, B.S.; Xiong, X.Y.; et al. Effect of Er and Si co-microalloying on mechanical properties and microstructures of AlCuMg alloys. *J. Mater. Res. Technol.* **2023**, *24*, 430–439. [CrossRef]

14. Liang, S.S.; Wei, W.; Wen, S.P.; Yuan, X.M.; Wu, X.L.; Huang, H.; Gao, K.Y.; Nie, Z.R. Enhanced thermal-stability of AlCuMg alloy by multiple microalloying segregation of Mg/Si/Sc solute. *Mater. Sci. Eng. A* **2022**, *831*, 142235. [CrossRef]

15. Marat, G.; Daniel, M.C.; Jesper, F.; Sigurd, W.; Randi, H.; Rustam, K. Precipitation behavior in an Al–Cu–Mg–Si alloy during ageing. *Mater. Sci. Eng. A* **2019**, *767*, 138369.

16. Li, J.; Chen, S.; Li, F.; Chen, K.; Huang, L. Synergy effect of Si addition and pre-straining on microstructure and properties of Al–Cu–Mg alloys with a medium Cu/Mg ratio. *Mater. Sci. Eng. A* **2019**, *767*, 138429. [CrossRef]

17. Patrick, S.; Jonathan, P.; Sumit, B.; Amit, S. The role of Si in determining the stability of the θ′ precipitate in Al-Cu-Mn-Zr alloys. *J. Alloys Compd.* **2021**, *862*, 158152.

18. Wolverton, C. Crystal structure and stability of complex precipitate phases in Al–Cu–Mg–(Si) and Al–Zn–Mg alloys. *Acta Mater.* **2001**, *49*, 3129–3142. [CrossRef]

19. Ringer, S.P.; Hono, K. Microstructural Evolution and Age Hardening in Aluminium Alloys: Atom Probe Field-Ion Microscopy and Transmission Electron Microscopy Studies. *Mater. Charact.* **2000**, *44*, 101–131. [CrossRef]

20. Liang, S.S.; Wen, S.P.; Wu, X.L.; Huang, H.; Gao, K.Y.; Nie, Z.R. The synergetic effect of Si and Sc on the thermal stability of the precipitates in AlCuMg alloy. *Mater. Sci. Eng. A* **2020**, *783*, 139319. [CrossRef]

21. Booth-Morrison, C.; Seidman, D.N.; Dunand, D.C. Effect of Er additions on ambient and high-temperature strength of precipitation-strengthened Al–Zr–Sc–Si alloys. *Acta Mater.* **2012**, *60*, 3643–3654. [CrossRef]

22. Yang, S.L.; Zhao, X.J.; Chen, H.W.; Wilson, N.; Nie, J.F. Atomic structure and evolution of a precursor phase of Ω precipitate in an Al-Cu-Mg-Ag alloy. *Acta Mater.* **2022**, *225*, 117538. [CrossRef]

23. Hu, S.Y.; Baskes, M.I.; Stan, M.; Chen, L.Q. Atomistic calculations of interfacial energies, nucleus shape and size of θ′ precipitates in Al–Cu alloys. *Acta Mater.* **2006**, *54*, 4699–4707. [CrossRef]

24. Shin, D.; Shyam, A.; Lee, S.; Yamamoto, Y.; Haynes, J.A. Solute segregation at the Al/θ′-Al2Cu interface in Al-Cu alloys. *Acta Mater.* **2017**, *141*, 327–340. [CrossRef]

25. Petrik, M.V.; Gornostyrev, Y.N.; Korzhavyi, P.A. Segregation of alloying elements to stabilize θ′ phase interfaces in Al-Cu based alloys. *Scr. Mater.* **2021**, *202*, 114006. [CrossRef]

26. Chen, H.; Yang, L.; Long, J. First-principles investigation of the elastic, Vickers hardness and thermodynamic properties of Al–Cu intermetallic compounds. *Superlattices Microstruct.* **2015**, *79*, 156–165. [CrossRef]

27. Wang, G.; Peng, L.; Li, K.; Zhu, L.; Zhou, J.; Miao, N.; Sun, Z. ALKEMIE: An intelligent computational platform for accelerating materials discovery and design. *Comput. Mater. Sci.* **2021**, *186*, 110064. [CrossRef]

28. Chong, X.; Hu, M.; Wu, P.; Shan, Q.; Jiang, Y.H.; Li, Z.L.; Feng, J. Tailoring the anisotropic mechanical properties of hexagonal M7X3 (M=Fe, Cr, W, Mo; X=C, B) by multialloying. *Acta Mater.* **2019**, *169*, 193–208. [CrossRef]

29. Zhang, D.L.; Wang, J.; Kong, Y.; Zou, Y.; Du, Y. First-principles investigation on stability and electronic structure of Sc-doped θ′/Al interface in Al−Cu alloys. *Trans. Nonferrous Met. Soc. China* **2021**, *31*, 3342–3355. [CrossRef]

30. Liu, L.H.; Chen, J.H.; Fan, T.W.; Liu, Z.R.; Zhang, Y.; Yuan, D.W. The possibilities to lower the stacking fault energies of aluminum materials investigated by first-principles energy calculations. *Comput. Mater. Sci.* **2015**, *108*, 136–146. [CrossRef]

31. Sheraz, A.; Sidra, B.S.; Muhammad, I.; Muhammad, A.; Kashif, K.M.; Jaehoon, K. Synthesis of long-chain paraffins over bimetallic Na–Fe0.9Mg0.1Ox by direct CO_2 hydrogenation. *Top. Catal.* **2024**, *67*, 363–376.

32. Sheraz, A.; Muhammad, I.; Wonjoong, Y.; Neha, K.; Rohmat, S.J.; Kashif, K.M.; Ki, K.S.; Jaehoon, K. Evaluation of MgO as a promoter for the hydrogenation of CO2 to long-chain hydrocarbons over Fe-based catalysts. *Appl. Catal. B Environ.* **2023**, *338*, 123052.

33. Liu, L.M.; Wang, S.Q.; Ye, H.Q. First-principles study of polar Al/TiN(1 1 1) interfaces. *Acta Mater.* **2004**, *52*, 3681–3688. [CrossRef]

34. Siegel Donald, J.; Hector Louis, G.; Adams James, B. First-principles study of metal–carbide/nitride adhesion: Al/VC vs. Al/VN. *Acta Mater.* **2002**, *50*, 619–631. [CrossRef]

35. Li, R.; Chen, Q.; Ouyang, L.; Ding, Y. Adhesion strength and bonding mechanism of γ-Fe (111)/α-Al2O3 (0001) interfaces with different terminations. *J. Alloys Compd.* **2021**, *870*, 159529. [CrossRef]

36. Aaronson, H.I.; Clark, J.B.; Laird, C. Interfacial energy of dislocation and of coherent interphase boundaries. *Met. Sci. J.* **1968**, *2*, 155–158. [CrossRef]

37. Gao, Y.H.; Guan, P.F.; Su, R.; Chen, H.W.; Yang, C.; He, C.; Cao, L.F.; Song, H.; Zhang, J.Y.; Zhang, X.F.; et al. Segregation-sandwiched stable interface suffocates nanoprecipitate coarsening to elevate creep resistance. *Mater. Res. Lett.* **2020**, *8*, 446–453. [CrossRef]

38. Bourgeois, L.; Dwyer, C.; Weyland, M.; Nie, J.F.; Muddle, B.C. Structure and energetics of the coherent interface between the θ′ precipitate phase and aluminium in Al–Cu. *Acta Mater.* **2011**, *59*, 7043–7050. [CrossRef]